Flow Dynamics of green sand in the DISAMATIC moulding process using Discrete element method (DEM)

Hovad, Emil; Larsen, P.; Walther, Jens Honore; Thorborg, Jesper; Hattel, Jesper Henri

Published in:
I O P Conference Series: Materials Science and Engineering

Link to article, DOI:
10.1088/1757-899X/84/1/012023

Publication date:
2015

Document Version
Publisher's PDF, also known as Version of record

Flow Dynamics of green sand in the DISAMATIC moulding process using Discrete element method (DEM)

2015 IOP Conf. Ser.: Mater. Sci. Eng. 84 012023

(http://iopscience.iop.org/1757-899X/84/1/012023)

Flow Dynamics of green sand in the DISAMATIC moulding process using Discrete element method (DEM)

E Hovad[1,3], P Larsen[3], J H Walther[1], J Thorborg[1,2] and J H Hattel[1]
1 Department of Mechanical Engineering, Technical University of Denmark (DTU)
2 MAGMA Giessereitechnologie GmbH, Kackertstr. 11, 52072 Aachen, Germany
3 DISA Industries A/S, Højager 8, 2630 Taastrup, Denmark

E-mail: emilh@mek.dtu.dk

Abstract. The DISAMATIC casting process production of sand moulds is simulated with DEM (discrete element method). The main purpose is to simulate the dynamics of the flow of green sand, during the production of the sand mould with DEM. The sand shot is simulated, which is the first stage of the DISAMATIC casting process. Depending on the actual casting geometry the mould can be geometrically quite complex involving e.g. shadowing effects and this is directly reflected in the sand flow during the moulding process. In the present work a mould chamber with "ribs" at the walls is chosen as a baseline geometry to emulate some of these important conditions found in the real moulding process. The sand flow is simulated with the DEM and compared with corresponding video footages from the interior of the chamber during the moulding process. The effect of the rolling resistance and the static friction coefficient is analysed and discussed in relation to the experimental findings.

1. Introduction

The DISAMATIC process is extensively used in casting of metal parts for the automotive industry for making breaking disks, crank shafts, engine blocks etc. In order to ensure a high quality of the components, it is important to control the manufacturing process of the mould, so that it is homogeneous and stable. A short explanation of the DISAMATIC process for manufacturing of the mould, is given in [1]. The following figure 1, is an illustration of the sand shot in the mould chamber. The flow dynamics of the sand shot inside the mould chamber is investigated with DEM and compared to the video footage, capturing the flow dynamics in the real mould chamber. The sand shot is driven by air pressure, initializing the flow of sand from the hopper above, into the chamber below. The sand fills out the mould geometry in the chamber at around the time 1 s.

Hence, the focus of the present work is on the sand shot and how this first part of the moulding process can be modelled numerically with the DEM, in this study only the sand phase is investigated. The first period of the sand shot 0.6 s is investigated, where the space underneath the three "ribs" is filled with green sand (see figure 3). Earlier research has been done, using DEM to simulate the sand flow [2] as well as the subsequent squeezing process [3] in the application of green sand moulding. Obtaining the right DEM parameters to realistically simulate the process is important, but at the same time also quite challenging [4]. This especially goes for the green sand material properties due to the small particle size around 0.2 mm as well as for the description of adhesion. The latter is often neglected in DEM simulations and this is also the case for the present work.

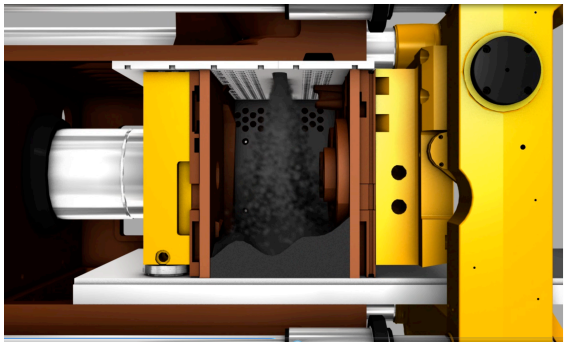

Figure 1. The sand shot, the sand coming from the hopper down into the chamber. The simulation of the sand shot is the topic of the present work.

DEM has also been used to simulate the lost foam process [5], where it was suggested that the rolling resistance and the Coulomb sliding friction are the most important parameters for the flow behaviour in this process. The fitting of rolling resistance and sliding friction parameters was studied in [4], in which different experimental tests were used for calibration. Particle scaling is frequently needed in the discrete element method [6], in this study two different particle sizes are used for the simulations.

2. Discrete element method (DEM).

DEM has received increased attention the last decade and the general application areas of the method can be found in e.g. [7]. A general review of the method's theoretical foundation is also given by [8] and a comparison of different frequently used DEM models was made by Di Renzo et. Al [9]. With the advancement in computational power and the introduction of parallel computing in DEM, the method also seems to be convenient for granular flow [10] and [11]. The commercial software STAR-CCM+ has been used for the 2-D simulations.

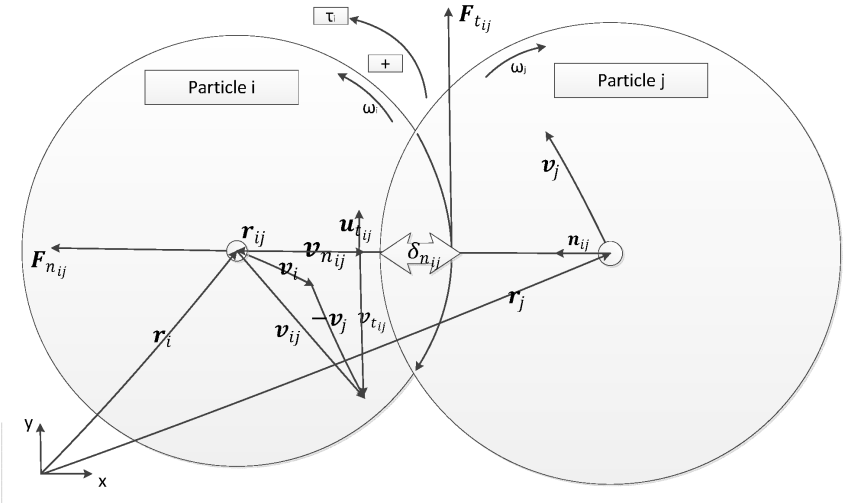

Figure 2. Particle i-th impact with particle j-th, the force exerted on the i-th particle in the normal direction is $\boldsymbol{F}_{n_{ij}}$ and in the tangential direction is $\boldsymbol{F}_{t_{ij}}$.

In figure 2, the impact distance $r_{ij} = \|\boldsymbol{r}_{ij}\|_2$ of the spherical i-th particle center of mass ($\boldsymbol{r}_i$) is found by the spherical particle j-th center of mass ($\boldsymbol{r}_j$) as

$$\boldsymbol{r}_{ij} = \boldsymbol{r}_i - \boldsymbol{r}_j \quad (1)$$

In DEM there is a normal direction ($\boldsymbol{n}_{ij} = \frac{\boldsymbol{r}_{ij}}{r_{ij}}$). The relative velocity of the two particles is

$$\boldsymbol{v}_{ij} = \boldsymbol{v}_i - \boldsymbol{v}_j$$

decomposed to a velocity in the normal direction ($\boldsymbol{v}_{n_{ij}}$) and a velocity in the tangential ($\boldsymbol{v}_{t_{ij}}$) to find the elastic force from the "spring" and the viscous damping force from the "dashpot" [11][12]. The normal velocity is given by

$$\boldsymbol{v}_{n_{ij}} = (\boldsymbol{n}_{ij} \cdot \boldsymbol{v}_{ij})\boldsymbol{n}_{ij} \quad (2)$$

The tangential velocity vector is defined as

$$\boldsymbol{v}_{t_{ij}} = \boldsymbol{v}_{ij} - \boldsymbol{v}_{n_{ij}} - (\boldsymbol{\omega}_i R_i + \boldsymbol{\omega}_j R_j) \times \boldsymbol{n}_{ij} \quad (3)$$

The normal displacement is $\delta_{n_{ij}} = \left\|\boldsymbol{v}_{n_{ij}}\right\|_2 \Delta t$ and the tangential displacement vector $\boldsymbol{u}_{t_{ij}}$ is found by integration of the tangential velocity $\frac{d\boldsymbol{u}_{t_{ij}}}{dt} = -\boldsymbol{v}_{t_{ij}}$

The simplified Hertz-Mindlin (H-MDns) force model with non-linear damping is used [13] [14] [15] and now that the displacements has been found the normal interaction force can be found

$$\boldsymbol{F}_{n_{ij}} = \boldsymbol{n}_{ij} K_n \delta_{n_{ij}}{}^{3/2} - N_n \boldsymbol{v}_{n_{ij}} \quad (4)$$

The tangential interaction force

$$\boldsymbol{F}_{t_{ij}} = \boldsymbol{u}_{t_{ij}} K_t - N_t \boldsymbol{v}_{t_{ij}} \quad (5)$$

K_n is the normal stiffness and K_t is the tangential stiffness, note that N_n is the normal and N_t the tangential non-linear damping model [13].

There is a max tangential force due to the Coulomb's law,

$$\left\|\boldsymbol{F}_{t_{ij}}\right\|_2 < \left\|\mu_s \boldsymbol{F}_{n_{ij}}\right\|_2 \quad (6)$$

μ_s is the static friction coefficient. Finally the total force on the particle is,

$$\boldsymbol{F}_i^{tot} = m_i \boldsymbol{g} + \sum_j (\boldsymbol{F}_{n_{ij}} + \boldsymbol{F}_{t_{ij}}) \quad (7)$$

The tangential forces give a final torque on the i-th particle,

$$\boldsymbol{T}_i = -R_i \sum_j \left(\boldsymbol{n}_{ij} \times \boldsymbol{F}_{t_{ij}}\right) \quad (8)$$

From this the acceleration, velocity and position is calculated by Newton second law, incrementally for each time step. The rolling resistance chosen is the Constant Torque Method first used by Zhou et. Al [16]. The relative rotation between the two particles is defined as $\boldsymbol{\omega}_{rel} = \boldsymbol{\omega}_i - \boldsymbol{\omega}_j$ and the Constant Torque Method is used to calculate the rolling resistance, defined as

$$\boldsymbol{T}_{\mathrm{rol}} = -\frac{\boldsymbol{\omega}_{rel}}{|\boldsymbol{\omega}_{rel}|} \mu_r R_{eq} \boldsymbol{F}_{n_{ij}} \quad (9)$$

So the tangential force $\boldsymbol{T}_i$ is counteracted by a torque from the rolling resistance $\boldsymbol{T}_{\mathrm{rol}}$ and the rolling resistance is μ_r.

3. Settings for the simulation

In the following figure 3, a simulation of the sand shot is shown with the green sand coming from top of the chamber with the flow rate and the initial velocity calculated from the experimental footage.

The flow rate is calculated by the circle diameter e.g. d=0.004 m, filling time 1.05 s, the assumed packing fraction of 0.75 and the total area of the mould which is $0.25\ m^2$ and finally this gives the flow rate $\frac{0.75 \cdot 0.25 m^2}{(0.002m)^2 \pi \cdot 1.05\ s} = 14210\ particles/s$. The diameter of 0.002 m gives the 56840 particles/s.

The particle velocity at the inlet is found by a simple 2-D bulk flow calculation based on the areas filling time of sand and orifice length from the actual chamber and experimental video footage.

This area has the height going to the third rib, $h = 0.3\ m$ (see figure 3) and the width of the chamber is $w = 0.48\ m$, then this area is $0.3\ m \cdot 0.48\ m = 0.144\ m^2$.

The orifice width is 0.04 m and the filling time of the area is around 0.6 s, so the average vertical velocity is estimated to be $v_y = \frac{0.144m^2}{0.04m \cdot 0.6\ s} = 6.0\ m/s$. For a more realistic velocity distribution a normal distribution is assumed around the calculated mean value and the standard deviations is given in table 1.

Table 1. The velocity distribution.

Direction	Mean value (m/s)	Standard deviation (m/s)	Velocity range Min (m/s)	Max (m/s)
v_x	0	0.1	-0.1	0.2
v_y	-6.0	0.1	-5.8	-6.2

The time step is chosen to be Δt=0.00001 s, plots of the velocities are made for every 500 time step, corresponding to the time 0.005 s, 0.01 s, 0.015 s and 0.02 s etc.

Table 2. Material values for the simulation.

Material properties	Value
Solid density – green sand	1600 kg/m3
Solid density – chamber wall	7500 kg/m3
Young's modulus – green sand	17000 MPa
Young's modulus – chamber wall	200000 MPa
Poisson ratio – green sand	0.3
Poisson ratio – chamber side	0.3
Coefficient of restitution particle-particle	0.01
Coefficient of restitution particle-wall	0.01
Gravity	9.82 m/s2

In table 2 typical values have been chosen for the Poisson ratio and Young modulus for the steel in the chamber wall. For the sand it is chosen to be the same value as a similar material, brick in STAR-CCM+. The sand in the mould has a density of 1200 kg/m^3 after the sand shot and before squeezing. The density of "representative" sand particles is $\frac{1200\ \mathrm{kg/m^3}}{0.75} = 1600\ \frac{\mathrm{kg}}{\mathrm{m^3}}$, due to the packing fraction.

The coefficient of restitution is chosen to be very small and very close to critical damping. This is due to the high damping properties of the bentonite coated green sand and Young modulus have been suggested to be of less importance compared to the rolling resistance (equation (9)) and static friction coefficient (equation (6)), [5].

Table 3. Simulation parameters, where the rolling resistance is μ_r and the static friction coefficient is μ_s.

Diameter	$\mu_{s,}$	μ_r	Injection rate
4 mm	0.8	0.6	14210 particles/s
4 mm	0.8	0.9	14210 particles/s
4 mm	1	0.6	14210 particles/s
4 mm	1	0.9	14210 particles/s
2 mm	0.8	0.6	56841 particles/s
2 mm	0.8	0.9	56841 particles/s
2 mm	1	0.6	56841 particles/s
2 mm	1	0.9	56841 particles/s

In table 3, choosing different values for the rolling resistance and static friction coefficient simulates changing the flow ability of the particles. This way, the effect of changing the moisture and bentonite content in the "real" green sand can be simulated as this changes the flow ability.

4. Results of simulation and experiment

The result that will be presented show when the flow front passes underneath the three "ribs" into the three "cavities" at the right side wall, seen in the following figure 3. The flow front is hard to define and track exactly in DEM, so six times intervals t_1-t_6 are constructed for the arrival of the particles at the six positions. These six times intervals t_1-t_6 will be measured for the flow front for different parameter values of the rolling resistance, static friction coefficient and particle radius and will then be compared to the experimental results.

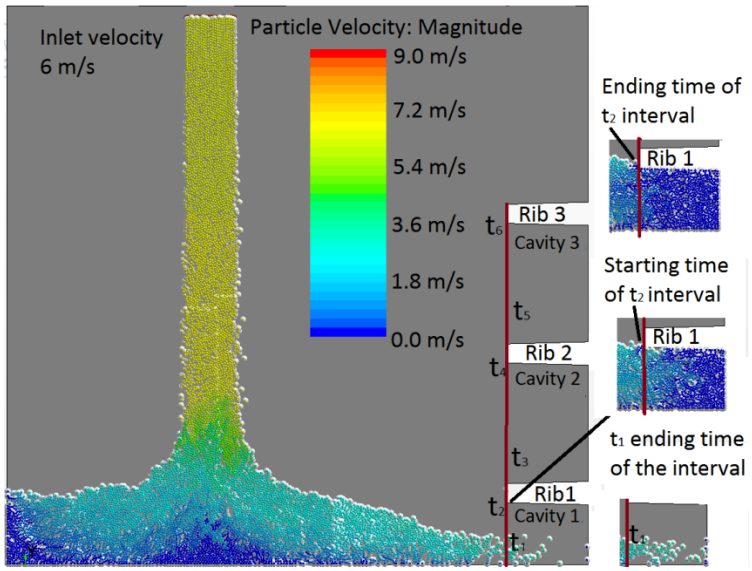

Figure 3. Tracking the front of the flow profile at the 6 different positions (t_1-t_6). An example of interval start and end time is shown in the bottom right corner of the figure for the time interval denoted t_1. An example of interval start and ending is shown in the right top of the figure for the time interval denoted t_2. The magnitude of the velocity is plotted with a scaling of 0-9 m/s the scale going from minimum dark blue, 0 m/s to the maximum velocity red 9 m/s.

In figure 3, the starting time for the interval, is when the flow front reaches the brown line and the ending time of the interval is when the bulk flow of the flow front has reached the brown line. The flow reaches the "cavities" underneath the three "ribs", when the particles cross the brown line into cavity 1 (t_1), cavity 2 (t_3) and cavity 3 (t_5). The starting time of the interval is when the "loosely packed particles" reach into the cavities and ending time of the interval is when the bulk flow or "closely packed particles" reach the cavities. The starting times of t_2, t_4 and t_6 intervals are when the flow front reaches the bottom edge of rib 1, 2 and 3 subsequently. Here the starting times of the time intervals are again when the "loosely packed" particles hit the bottom edge of the rib in the time step. The ending time of t_2, t_4 and t_6 intervals are again defined as when the "closely packed particles" reaches the bottom edge rib in the time step. The following table 4 will show all the intervals t_1-t_6 for

the different simulations and selected plots will be made showing the flow profile passing the different positions and compared to the video footage.

Table 4. The six time intervals t_1-t_6, where each interval (start-end) indicates the period, when the flow front reaches the selected positions at the brown line. The experimental values are shown in the last row.

Simulations values	t_1 [s]	t_2 [s]	t_3 [s]	t_4 [s]	t_5 [s]	t_6 [s]
μ_r=0.6, μ_r=0.8, 4 mm	0.155-0.170	0.215-0.225	0.255-0.270	0.380-0.390	0.435-0.445	0.585-0.590
μ_r=0.9, μ_r=0.8, 4 mm	0.175-0.205	0.225-0.245	0.275-0.290	0.380-0.390	0.450-0.460	0.585-0.600
μ_r=0.6, μ_r=1, 4 mm	0.160-0.165	0.225-0.230	0.250-0.260	0.385-0.395	0.440-0.450	0.590-0.605
μ_r=0.9, μ_r=1, 4 mm	0.175-0.185	0.235-0.240	0.255-0.270	0.410-0.420	0.475-0.480	0.625-0.665
μ_r=0.6, μ_r=0.8, 2 mm	0.145-0.155	0.215 -0.220	0.245-0.250	0.370-0.380	0.415-0.425	0.550-0.560
μ_r=0.9, μ_r=0.8, 2 mm	0.155-0.165	0.220-0.225	0.240-0.245	0.380-0.390	0.435-0.440	0.585-0.595
μ_r=0.6, μ_r=1, 2 mm	0.150-0.165	0.210-0.215	0.235-0.240	0.365-0.370	0.440-0.450	0.540-0.550
μ_r=0.9, μ_r=1, 2 mm	0.155-0.160	0.215-0.225	0.240-0.250	0.380-0.385	0.430-0.440	0.590-0.595
Experiment	0.254-0.262	0.304-0.313	0.325-0.342	0.429-0.441	0.467-0.492	0.575-0.591

In table 4, the different values for the six time intervals t_1-t_6 are listed for the different simulations values and the experiment. A mean is calculated for each of the two diameters overall simulation times, this includes all the 4 times interval for each of the six columns with the times intervals t_1-t_6. Maximum and minimum times are also found from the 4 times interval for each of the six columns with the times intervals t_1-t_6. So for all the simulations with the diameter e.g d=4, a mean, maximum and minimum is calculated for each of the six time intervals t_1-t_6. The results from table 4 are depicted in figure 4, with the mean, maximum and minimum values plotted for the two diameters and the experiment.

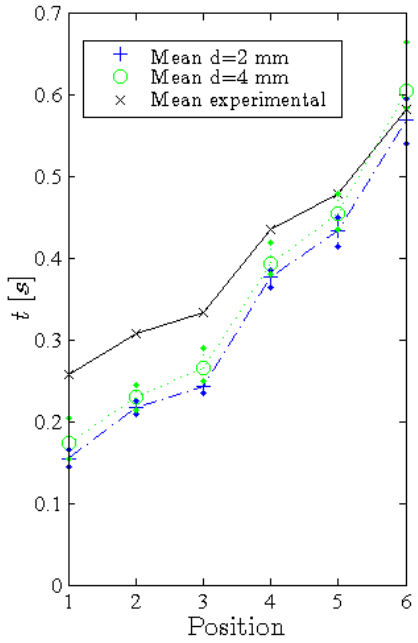

Figure 4. The mean, maximum and minimum times for t_1-t_6 for all the simulations compared to the experiment. The solid black line is linear interpolation of the experimental mean; the cross is the actual value of the experimental mean. The circle is the mean of the diameter d=4 mm and the plus is the diameter d=2 mm. The green dots are the intervals minimum and maximum of the diameter 4 mm and the blue dots represents the diameter 2 mm.

In figure 4, the simulation of diameter 4 mm mean is occurring around 0.06 s earlier than the first times t_1-t_3 from the experimental mean's and the difference narrows as the flow passes at the times t_4–t_5, at t_6 the simulations reached this point later than the experiment. Similarly dynamics occurs for the simulation of diameter 2 mm, where the mean is occurring around 0.08 s earlier compared to the experimental mean, for the first times t_1-t_3 and the difference narrows as the flow passes at the times t_4–t_5 and at the time t_6 the simulations are very close to the experimental value (difference 0.01). The larger diameters of 4 mm, have longer t_1-t_6 times than the diameter of 2 mm. The specific simulation chosen is the diameter of 2 mm, rolling resistance μ_r=0.9 and static friction coefficient μ_s=1, because this simulation's qualitative flow dynamics is very similar to the experiment. In figure 5 (simulation) and figure 6 (experiment) the progression of the flow front at t_2 is presented and the results are compared. The flow profile of the experiment figure 6, shows a quite conical pile shape (free surface shape) and the simulation exhibits a very similar conical shaped flow profile, although the actual time of the occurrence (t_2) is somewhat different i.e. 0.1 s, as earlier mentioned.

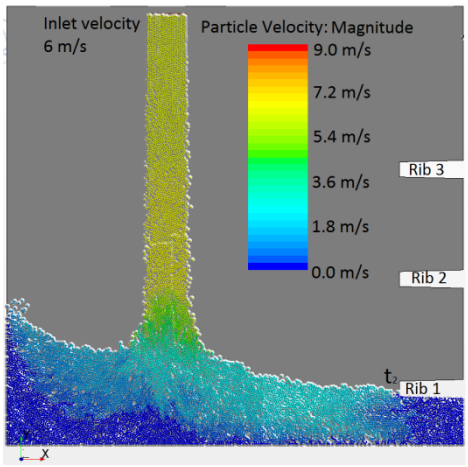

Figure 5. The simulation in the interval of t_2 plot taken at the time 0.225 s (μ_r=0.9, μ_s=1, 2 mm).

Figure 6. The experiment: t_2 at the time of 0.32 s, the contour of the flow profile can be seen on the rear wall.

5. Conclusion

The sand shot in the DISAMATIC process has been investigated with experimental video footage of the chamber and also simulated with DEM "representing" the sand particles. The dynamical flow properties of the green sand have been quantified by tracking the flow fronts arrival in six positions for the "ribbed" geometry. The Experimental video footage flow front and the DEM simulations flow front are compared for these six filling positions in the times (t_1-t_6) and plotted together with mean, minimum and maximum values. Selected plot for a specific chosen simulation is compared with the experimental footage, when the flow fronts has reached the rib 1 bottom edge position (t_2) and these flow fronts profiles similarities is discussed.

The main findings of the discrete element method for modelling green sand flow during production of DISA moulds is presented below.

- The dynamic flow behaviour of the particles in the simulation is similar to the experiment
- The behaviour of the time intervals (t_1-t_6) for the simulation is also similar to the experiment

- The flow ability changes to a more viscous flow with larger rolling resistance and static friction coefficient, resembling the behaviour of moisture and bentonite content in green sand
- With the correct particle velocity, flow rate, damping coefficient, rolling resistance and static friction coefficient it is possible to simulate the experimental video footage very well

The experimental data t_1 is slower with a time delay of 0.1 s for the diameter 2 mm and 0.8 s for the diameter 4 mm compared to these simulations, properly due to a non-constant flow rate in the inlet, especially overestimating the initial flow rate. In later studies the flow rate will be fitted more precisely with the experimental video footage and selected material values will also be tested experimentally. The density will also be measured from experiments and compared to the simulations. Overall it is possible to represent the flow quite well with a DEM model especially qualitative behaviors of the flow and for the different times t_1-t_6.

References

[1] DISA Industries A/S 2013 DISA 231/DISA 231 Var. Sand Moulding System Instructions for Use
[2] Makino H, Maeda Y and Nomura H 2002 Computer Simulation of Various Methods for Green Sand Filling *Trans. Am. Foundry Soc.* **110** 1–9
[3] Maeda Y, Maruoka Y, Makino H and Nomura H 2003 Squeeze molding simulation using the distinct element method considering green sand properties *J. Mater. Process. Technol.* **135** 172–8
[4] Grima A P and Wypych P W 2011 Discrete element simulations of granular pile formation: Method for calibrating discrete element models *Eng. Comput.* **28** 314–39
[5] Rojek J, Zarate F, de Saracibar C A, Gilbourne C and Verdot P 2005 Discrete element modelling and simulation of sand mould manufacture for the lost foam process *Int. J. Numer. Methods Eng.* **62** 1421–41
[6] Sakai M, Takahashi H, Pain C C, Latham J-P and Xiang J 2012 Study on a large-scale discrete element model for fine particles in a fluidized bed *Adv. Powder Technol.* **23** 673–81
[7] Zhu H P, Zhou Z Y, Yang R Y and Yu A B 2008 Discrete particle simulation of particulate systems: A review of major applications and findings *Chem. Eng. Sci.* **63** 5728–70
[8] Zhu H P, Zhou Z Y, Yang R Y and Yu a. B 2007 Discrete particle simulation of particulate systems: Theoretical developments *Chem. Eng. Sci.* **62** 3378–96
[9] Di Renzo A and Di Maio F P 2004 Comparison of contact-force models for the simulation of collisions in DEM-based granular flow codes *Chem. Eng. Sci.* **59** 525–41
[10] Cleary P W 2009 Industrial particle flow modelling using discrete element method *Eng. Comput.* **26** 698–743
[11] Walther J H and Sbalzarini I F 2009 Large-scale parallel discrete element simulations of granular flow *Eng. Comput.* **26** 688–97
[12] Cundall P A and Strack O D L 1979 A discrete numerical model for granular assemblies *Géotechnique* **29** 47–65
[13] Tsuji Y, Tanaka T and Ishida T 1992 Lagrangian numerical simulation of plug flow of cohesionless particle in a horizontal pipe *Powder Technol.* **71** 239–50
[14] Hertz H 1881 Über die Berührung fester elastischer Körper *J. für die reine und Angew. Math.* **171** 156–71
[15] Mindlin R D and Deresiewicz H 1953 Elastic spheres in contact under varying oblique forces *Am. Soc. Mech. Eng. -- Trans. -- J. Appl. Mech.* **20** 327–44
[16] Zhou Y C, Wright B D, Yang R Y, Xu B H and Yu a. B 1999 Rolling friction in the dynamic simulation of sandpile formation *Phys. A Stat. Mech. its Appl.* **269** 536–53